

# Eigenstate Thermalization for Local versus Translationally Invariant Observables

Rohit Patil and Marcos Rigol

*Department of Physics, The Pennsylvania State University, University Park, Pennsylvania 16802, USA*

Local observables and their translationally invariant counterparts are generally thought as providing the same predictions for experimental measurements. This is used in the context of their expectation values, which are indeed the same in clean systems (up to finite-size effects), but also in the context of their correlation functions, which need not be the same. We examine this intuition from the perspective of the eigenstate thermalization hypothesis. Specifically, we explore the diagonal matrix elements and the spectral functions of local and translationally invariant observables in the spin-1 tilted field Ising chain with periodic and open boundary conditions. We discuss in which ways those observables are different and in which contexts they can be thought as being the same. Furthermore, we unveil a novel form of off-diagonal eigenstate thermalization in translationally invariant systems that applies to pairs of energy eigenstates with different quasimomenta.

*Introduction.* In experiments, one is usually interested in probing local observables within the bulk of materials of interest, e.g., charge and/or spin correlations in a high-temperature superconductor [1], etc. Those systems have a finite extent and “open boundary conditions” (OBCs) yet, when the effects of disorder and imperfections can be neglected, in theoretical calculations we usually consider simplified translationally-invariant models with periodic boundary conditions (PBCs). In those models quasimomentum is conserved so that, e.g., for noninteracting electrons one has a well-defined band structure that can be used to understand traditional metals and insulators. To take full advantage of translational invariance, instead of theoretically studying local observables one usually studies their translationally invariant sums. This simplifies analytical derivations and makes possible the study of larger systems in numerical calculations.

Differences in the boundary conditions are important when one is interested in edge or surface effects, e.g., in topological insulators [2], can result in subtleties when studying transport properties, e.g., the Drude weight [3, 4], and can change the scaling of finite-size effects in numerical calculations [5]. They have been discussed in different contexts in the literature. In this work we explore the differences between local observables and their translationally invariant counterparts in the context of the eigenstate thermalization hypothesis (ETH) for clean systems with OBCs as well as with PBCs.

In generic isolated quantum systems, the equilibration of observables to their thermal equilibrium values is understood to be a consequence of eigenstate thermalization. The corresponding mathematical ansatz for the matrix elements  $O_{mn} \equiv \langle \psi_m | \hat{O} | \psi_n \rangle$  of an observable  $\hat{O}$  in the eigenbasis  $\{|\psi_m\rangle\}$  of a quantum-chaotic Hamiltonian  $\hat{H}$  ( $\hat{H}|\psi_m\rangle = E_m|\psi_m\rangle$ ), is known as the ETH [6–10]:

$$O_{mn} = O(E_m)\delta_{mn} + e^{-\frac{S(\bar{E}_{mn})}{2}} f_O(\bar{E}_{mn}, \omega_{mn}) R_{mn}^O, \quad (1)$$

where  $\bar{E}_{mn} = (E_m + E_n)/2$  is the average energy,  $\omega_{mn} = E_m - E_n$  is the energy difference,  $O(E_m)$  and  $f_O(\bar{E}_{mn}, \omega_{mn})$  are smooth functions,  $S(\bar{E}_{mn})$  is the thermodynamic entropy at the energy  $\bar{E}_{mn}$ , and  $R_{mn}^O$  are

close to normal distributed random numbers with zero mean and unit variance (variance 2) for  $m \neq n$  ( $m = n$ ) in systems with time-reversal symmetry. The ETH (1), which characterizes the first two moments of the distribution of  $O_{mn}$ , has been extended to include correlations needed to describe quantities involving higher moments [11, 12], like the out-of-time-order correlators [11, 13–17]. Correlations have also been advanced between matrix elements of different observables [10–12, 18]. Those are behind our findings in this study.

In the grand-canonical ensemble, the expectation value of an observable  $\hat{O}$  at inverse temperature  $\beta$  can be written as  $O(\beta) = \frac{1}{Z} \text{Tr}(\hat{O} e^{-\beta \hat{H}})$ , where  $Z = \text{Tr}(e^{-\beta \hat{H}})$ , and  $\hat{H}$  is the Hamiltonian. The corresponding average energy is  $E(\beta) = \frac{1}{Z} \text{Tr}(\hat{H} e^{-\beta \hat{H}})$ . Using the ETH ansatz (1), we find that  $\hat{O}(\beta) \simeq O(E_m = E(\beta))$ , where the difference between the two in general vanishes polynomially with system size [10]. We are interested in the properties of local observables  $\hat{O}^j$ , at site  $j$  of chains with  $L$  sites, and their translationally invariant (intensive) counterparts

$$\hat{\mathcal{O}} \equiv \frac{1}{L} \sum_{j=1}^L \hat{O}^j. \quad (2)$$

In the presence of translational symmetry,  $O_{mm}^j = O_{mm}^l \forall j, l$  so  $\mathcal{O}_{\text{PBC}}(\beta) = O_{\text{PBC}}^j(\beta)$  [19]. On the other hand, for clean systems with OBCs,  $\mathcal{O}_{\text{OBC}}(\beta) \simeq O_{\text{OBC}}^j(\beta)$  [19] for  $j$  in the bulk. Finally,  $\mathcal{O}_{\text{OBC}}(\beta) \simeq \mathcal{O}_{\text{PBC}}(\beta)$ , and their difference in general vanishes polynomially with  $L$  [5]. These facts are behind the interchangeable use of local observables and their translationally invariant counterparts, as well as of PBCs and OBCs.

*Hamiltonian and diagonal ETH.* We study the spin-1 tilted-field Ising model in chains with PBCs and OBCs:

$$\hat{H}_{\text{PBC}} = J \sum_{j=1}^L \hat{S}_z^j \hat{S}_z^{j+1} + h_x \sum_{j=1}^L \hat{S}_x^j + h_z \sum_{j=1}^L \hat{S}_z^j, \quad (3)$$

$$\hat{H}_{\text{OBC}} = \hat{H}_{\text{PBC}} - J \hat{S}_z^L \hat{S}_z^1 + 0.1 \hat{S}_z^1, \quad (4)$$

where  $\hat{S}_\gamma^j$  is the spin-1 operator along the  $\gamma \in \{x, y, z\}$  direction at site  $j$ . We take  $J = 0.707$ ,  $h_x = 1.1$ , and

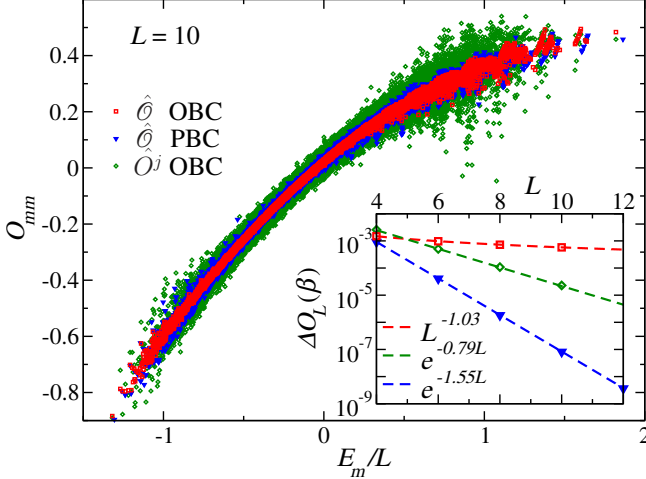


FIG. 1. Diagonal matrix elements  $O_{mm}$  vs the energy density  $E_m/L$  for the local observable  $\hat{O}^j = \hat{S}_x^j$  at site  $j = \frac{L}{2}$  for OBCs, and its translationally invariant counterpart  $\hat{\mathcal{O}} = \frac{1}{L} \sum_j \hat{S}_x^j$  for OBCs and PBCs, in chains with  $L = 10$ . (Inset) Relative difference  $\Delta O_L(\beta)$  between  $O_L(\beta)$  in a chain with  $L$  sites and its thermodynamic limit value  $O_{TL}(\beta)$  for  $\beta = 0.5$ , see text.  $O_{TL}(\beta)$  is obtained fitting the PBC results for the largest four chains to  $O_L(\beta) = O_{TL}(\beta) + ae^{-bL}$  with fitting parameters  $O_{TL}(\beta)$ ,  $a$ , and  $b$ . That value is used for OBCs to fit  $\Delta O_L(\beta)$  for  $\hat{O}^j$  to  $ae^{-bL}$ , and for  $\hat{\mathcal{O}}$  to  $aL^{-b}$ , with fitting parameters  $a$  and  $b$ . The fits are shown as lines.

$h_z = 0.9$  for the model to be nonintegrable [20]. In chains with OBCs (4), we add a weak field in the first site along  $z$  to break the lattice reflection symmetry. We study the local observable  $\hat{O}^j = \hat{S}_x^j$  at site  $j = [L/2]$  and its translationally invariant counterpart  $\hat{\mathcal{O}} = \frac{1}{L} \sum_{j=1}^L \hat{S}_x^j$  [21].

In Fig. 1 we plot the diagonal matrix elements  $O_{mm}$  versus the energy density  $E_m/L$  for  $\hat{O}^j$  and  $\hat{\mathcal{O}}$  in chains with OBCs, and for  $\hat{\mathcal{O}}$  in chains with PBCs. The results are consistent with the ETH in all three cases, but the magnitudes of the eigenstate to eigenstate fluctuations depend on the observable and the boundary conditions. Those fluctuations are similar for  $\hat{\mathcal{O}}$  independently of the boundary conditions, are largest for  $\hat{O}^j$  in chains with OBCs, and we verified that they decrease exponentially with system size in all cases (not shown). To quantify how the grand-canonical expectation values in finite chains  $O_L(\beta)$  converge to the thermodynamic limit result  $O_{TL}(\beta)$ , we compute the relative difference  $\Delta O_L(\beta) = |O_L(\beta) - O_{TL}(\beta)|/|O_{TL}(\beta)|$ . As shown in the inset in Fig. 1, the relative difference for  $\hat{\mathcal{O}}$  decreases exponentially fast for PBCs and polynomially fast for OBCs [5]. Remarkably, for  $\hat{O}^j$  with  $j$  at the center of the chain, the decrease is exponentially fast for OBCs. This indicates that so long as one is interested in the bulk expectation values of local observables, it does not matter (up to finite-size effects) whether one computes those observables or their translationally invariant counterparts in chains with OBCs or PBCs.

*Spectral function.* We explore next the off-diagonal matrix elements, focusing on the spectral functions at “infinite temperature”, i.e., for  $E_\infty \equiv E(\beta = 0) = \frac{1}{D} \text{Tr}(\hat{H})$ , where  $D = 3^L$  is the Hilbert space dimension. For the observables  $\hat{O} = \hat{O}^j$  and  $\hat{\mathcal{O}}$  (2), we compute them as:

$$|f_{O^j}(E_\infty, \omega)|^2 = \frac{1}{D} \sum_{m,n \neq m} |O_{mn}^j|^2 \delta(\omega - \omega_{mn}), \quad (5)$$

$$|f_{\mathcal{O}}(E_\infty, \omega)|^2 = \frac{L}{D} \sum_{m,n \neq m} |\mathcal{O}_{mn}|^2 \delta(\omega - \omega_{mn}), \quad (6)$$

see, e.g., Refs. [20, 22–25], where the factor of  $L$  in Eq. (6) is a consequence of the Hilbert-Schmidt norm of  $\hat{\mathcal{O}}$  [26, 27]. We use the regularization  $\delta(x) \rightarrow \frac{1}{\sqrt{2\pi\sigma^2}} \exp(-\frac{x^2}{2\sigma^2})$  [25], with  $\sigma = 0.1\omega_H$ , where  $\omega_H$  is the average level spacing in the central 50% of the spectrum.

**OBCs.** We first study the spectral functions in chains with OBCs. The lack of symmetries of  $\hat{H}$  (4) means that the ETH is valid across the entire energy spectrum so that the spectral functions, which are well defined even if the ETH does not apply, e.g., in integrable systems [23, 28], correspond to  $|f_O(E_\infty, \omega)|^2$  in the ETH ansatz (1).

In Fig. 2, we show  $|f_{O^j}(E_\infty, \omega)|^2$  and  $|f_{\mathcal{O}}(E_\infty, \omega)|^2$  in the eigenstates of Hamiltonian (4). The two are quantitatively different but exhibit qualitatively similar behaviors: (i) at low frequencies they both develop the plateaus expected in nonintegrable systems below the Thouless energy [10], and (ii) at high frequencies they exhibit a fast decay. To understand the origin of their difference, we note that in Eq. (6) we can split:

$$|\mathcal{O}_{mn}|^2 = \frac{1}{L^2} \left[ \sum_{j=1}^L |O_{mn}^j|^2 + \sum_{\substack{j,l=1 \\ j \neq l}}^L O_{mn}^j (O_{mn}^l)^* \right]. \quad (7)$$

Hence, if  $R_{mn}^{O^j}$  and  $R_{mn}^{O^l}$  in Eq. (1) for  $j \neq l$  are uncorrelated (like in random matrix theory [10]), then for  $m \neq n$  the average over the matrix elements  $\overline{O_{mn}^j (O_{mn}^l)^*} = 0$ . Also, if  $|O_{mn}^j|^2$  are approximately the same in all sites in the bulk of the system, then  $\overline{|\mathcal{O}_{mn}|^2} \approx \frac{1}{L} \overline{|O_{mn}^j|^2}$ . In this case the spectral functions from Eqs. (5) and (6) are approximately the same. The differences between  $|f_{O^j}(E_\infty, \omega)|^2$  and  $|f_{\mathcal{O}}(E_\infty, \omega)|^2$  in clean systems with OBCs therefore signal the existence of correlations between the matrix elements of  $\hat{O}^j$  in different sites that are beyond the traditional random matrix theory formulation of the ETH. This is explicitly shown in the inset in Fig. 2, where we plot the contributions to  $|f_{\mathcal{O}}(E_\infty, \omega)|^2$  from terms with different values of  $|j - l|$  in Eq. (7). Those contributions depend on  $|j - l|$  and can be negative for  $j \neq l$ . The relative ordering between  $|f_{\mathcal{O}}(E_\infty, \omega)|^2$  and  $|f_{O^j}(E_\infty, \omega)|^2$  is observable dependent. For some observables, like  $\hat{S}_x$  considered here, they result in  $|f_{\mathcal{O}}(E_\infty, \omega)|^2 < |f_{O^j}(E_\infty, \omega)|^2$  at low frequencies, while for others  $|f_{\mathcal{O}}(E_\infty, \omega)|^2 > |f_{O^j}(E_\infty, \omega)|^2$  [21].

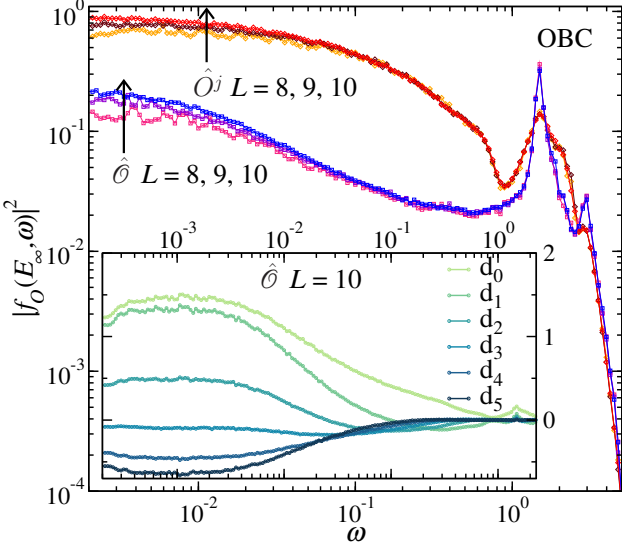


FIG. 2. Spectral functions for the local observable  $\hat{O}^j = \hat{S}_x^j$  at site  $j = [L/2]$  and its translationally invariant counterpart  $\hat{O} = \frac{1}{L} \sum_j \hat{S}_x^j$  in chains with OBCs (4). (Inset) Contributions to  $|f_{\hat{O}}(E_{\infty}, \omega)|^2$ , see Eq. (7), from terms with  $|j - l| = 0$  through 5 ( $d_0$  through  $d_5$  in the legend) in chains with  $L = 10$ .

The fact that the spectral functions  $|f_{\hat{O}}(E_{\infty}, \omega)|^2$  and  $|f_{O^j}(E_{\infty}, \omega)|^2$  are in general different can be understood studying systems with PBCs, as we explain next.

**PBCs.** We begin our discussion of systems with PBCs by stressing that, being well-defined physical quantities, the spectral functions of local operators and of their translationally invariant counterparts are (up to finite-size effects) independent of the boundary conditions. In Fig. 3, we show results for  $|f_{O^j}(E_{\infty}, \omega)|^2$  [Fig. 3(a)] and  $|f_{\hat{O}}(E_{\infty}, \omega)|^2$  [Fig. 3(b)] in chains with PBCs and OBCs and the same number of lattice sites ( $L = 10$ ). The results for  $|f_{O^j}(E_{\infty}, \omega)|^2$  are indistinguishable between OBCs and PBCs [Fig. 3(a)], while small differences are visible for  $|f_{\hat{O}}(E_{\infty}, \omega)|^2$  [Fig. 3(b)] because of the boundary effects in the small chains that we have diagonalized. Note that the log-linear scale used in the plots makes

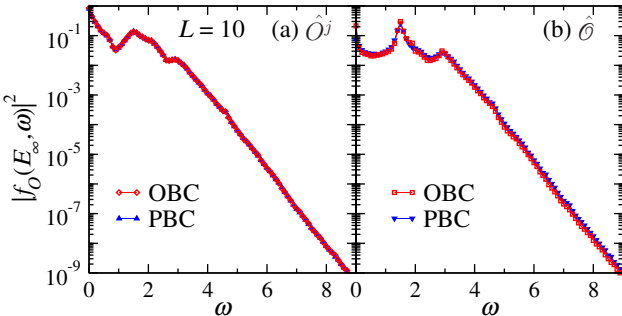


FIG. 3. Spectral functions for: (a)  $\hat{O}^j = \hat{S}_x^j$  at site  $j = L/2$ , and (b) its translationally invariant counterpart  $\hat{O} = \frac{1}{L} \sum_j \hat{S}_x^j$  in chains with PBCs and OBCs, and  $L = 10$ .

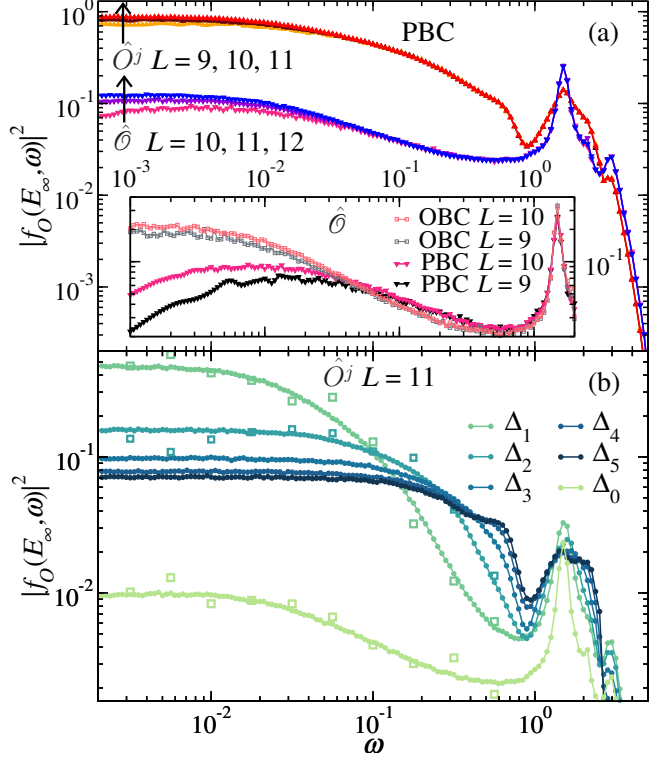


FIG. 4. (a) Spectral functions for  $\hat{O}^j = \hat{S}_x^j$  at site  $j = [L/2]$  and its translationally invariant counterpart  $\hat{O} = \frac{1}{L} \sum_j \hat{S}_x^j$  in chains with PBCs (3). (inset)  $|f_{\hat{O}}(E_{\infty}, \omega)|^2$  in chains with OBCs and PBCs for  $L = 9, 10$ . (b) Contributions to  $|f_{O^j}(E_{\infty}, \omega)|^2$  from the six terms with different values of  $\Delta_{\ell}$  in Eq. (10) for  $L = 11$ . Open squares represent the rescaled ETH functions  $\frac{1}{L} |f_{O^j}|^2$  ( $\frac{2}{L} |f_{O^j}|^2$ ) in Eq. (11) calculated using 100 pairs of states with  $E_{mn} \simeq E_{\infty}$  and  $\omega_{mn} \simeq \omega$  in blocks with quasimomenta  $k_m = \frac{2\pi}{L}$  and  $k_n = \frac{4\pi}{L}, \frac{6\pi}{L}$ .

apparent that the spectral functions decay exponentially fast with  $\omega$  [28]. In Fig. 4(a), we plot in log-log scale (to emphasize the low-frequency behavior of) the spectral functions of  $\hat{O}^j$  and  $\hat{O}$  for the three largest chains with PBCs (3) that we diagonalized. As expected, those results resemble the ones for OBCs shown in Fig. 2.

In translationally invariant chains (3) the differences between  $|f_{\hat{O}}(E_{\infty}, \omega)|^2$  and  $|f_{O^j}(E_{\infty}, \omega)|^2$  can be understood using the symmetry constraints. The eigenkets of the Hamiltonian  $\hat{H}$  (3) are simultaneous eigenkets of the single-site lattice translation operator  $\hat{T}$ , i.e.,  $\hat{T} |E_m, k_m\rangle = E_m |E_m, k_m\rangle$  and  $\hat{T}^* |E_m, k_m\rangle = e^{-ik_m} |E_m, k_m\rangle$ , with eigenenergy  $E_m$  and quasimomentum  $k_m = \frac{2\pi}{L} \eta_m$  (we set  $\hbar = 1$  and the lattice spacing  $a = 1$ ), where  $\eta_m = \eta_{\min}, \eta_{\min} + 1, \dots, \eta_{\max}$  with  $\eta_{\max} = -\eta_{\min} + 1 = \frac{L}{2}$  ( $\eta_{\max} = -\eta_{\min} = \lfloor \frac{L}{2} \rfloor$ ) for  $L$  even (odd). This means that, for any observable  $\hat{O}$ , the matrix  $O_{mn} \equiv \langle E_m, k_m | \hat{O} | E_n, k_n \rangle$  has  $L^2$  blocks of about the same size (with  $\sim \frac{D^2}{L^2}$  matrix elements) defined by the values of  $k_m$  and  $k_n$ . Next we note that since local operators at two different sites in a periodic chain are

related by a translation,  $\hat{O}^l = (\hat{T}^\dagger)^{(j-l)} \hat{O}^j (\hat{T})^{(j-l)}$ , their matrix elements are related via:

$$O_{mn}^l = O_{mn}^j e^{i(j-l)(k_m - k_n)}. \quad (8)$$

This implies that: (i) for  $k_m = k_n$ ,  $O_{mn}^j = O_{mn}^l \forall j, l$  so that  $\mathcal{O}_{mn} = O_{mn}^j \forall j$ , and (ii)  $\mathcal{O}_{mn} = 0$  for  $k_m \neq k_n$ .

Consequently, for the spectral function of translationally invariant operators  $\hat{O}$  in Eq. (6), the translational symmetry restricts the sums over  $n$  and  $m$  to pairs of energy eigenstates with the same quasimomentum:

$$|f_{\mathcal{O}}(E_\infty, \omega)|^2 = \frac{L}{D} \sum_{\substack{m, n \neq m \\ k_m = k_n}} |\mathcal{O}_{mn}|^2 \delta(\omega - \omega_{mn}). \quad (9)$$

The spectral function for local operators, on the other hand, also has contributions from pairs of energy eigenkets with different quasimomenta. Motivated by Eq. (9), we rewrite Eq. (5) grouping all contributions from energy eigenstates with the same value of  $|k_m - k_n| = \Delta_\ell$ , with  $\Delta_\ell = \frac{2\pi}{L}\ell$  and  $\ell = 0, 1, \dots, \lfloor \frac{L}{2} \rfloor$ :

$$|f_{O^j}(E_\infty, \omega)|^2 = \frac{1}{D} \sum_{\ell=0}^{\lfloor \frac{L}{2} \rfloor} \sum_{\substack{m, n \neq m \\ k_m = k_n \pm \Delta_\ell}} |O_{mn}^j|^2 \delta(\omega - \omega_{mn}). \quad (10)$$

The terms in Eq. (10) with  $\Delta_\ell = 0$  add to  $\frac{1}{L}|f_{\mathcal{O}}(E_\infty, \omega)|^2$ , because of the prefactor  $L$  in Eq. (9). This makes apparent that they have a vanishing (as  $\frac{1}{L}$ ) contribution to  $|f_{O^j}(E_\infty, \omega)|^2$ . Therefore, in the thermodynamic limit,  $|f_{O^j}(E_\infty, \omega)|^2$  is determined by the terms with  $\Delta_\ell \neq 0$ . Since there is no reason for those terms to add to  $L - 1$  times the sum for  $\Delta_\ell = 0$ , we conclude that, in general,  $|f_{\mathcal{O}}(E_\infty, \omega)|^2$  and  $|f_{O^j}(E_\infty, \omega)|^2$  are different in translationally invariant systems. This, together with the equivalence of the spectral functions in systems with PBCs and OBCs, implies that the correlations we observed between the matrix elements of local operators at different sites in systems with OBCs must exist in general.

In Fig. 4(b), we plot the contributions of the terms with the six different values of  $\Delta_\ell$  in Eq. (10) to the spectral function of  $\hat{O}^j$  for  $L = 11$ . They comply with our expectation of being different depending on the value of  $\Delta_\ell$ . For  $\Delta_\ell \neq 0$ , they exhibit a monotonic and physically meaningful behavior with increasing  $\Delta_\ell$ . The results for  $\Delta_1$  through  $\Delta_5$ , from top to bottom, show that the onset of the low-frequency plateau moves to higher frequencies as  $\Delta_\ell$  increases, which reflects that the longest time scales in the dynamics of  $\hat{O}^j$  associated to any given  $\Delta_\ell$  decrease with increasing  $\Delta_\ell$ , as expected for a shortening length scale  $\propto \frac{1}{\Delta_\ell}$ . The contribution from terms with  $\Delta_\ell = 0$  is special as there is no length scale associated to it. At low frequencies, as shown in the inset of Fig. 4(a), this results in differences between  $|f_{\mathcal{O}}(E_\infty, \omega)|^2$  in systems with PBCs and OBCs. In the latter,  $L$  is the longest length scale and

$|f_{\mathcal{O}}(E_\infty, \omega)|^2$  is similar at low frequency to the curve for  $\Delta_{\ell=1} = \frac{2\pi}{L}$  in Fig. 4(b), which is the contribution from the longest finite length scale for PBCs.

Our results in Fig. 4(b) beg the question of whether there is a formulation of the ETH in translationally invariant systems beyond Eq. (1), which applies to translationally invariant operators within each quasimomentum sector [29], given that local operators were already found to have dense Gaussian distributed matrix elements for  $k_m \neq k_n$  [30]. Generalizations of the ETH have been recently explored in the context of continuous non-Abelian symmetries [31–34]. In contrast to continuous symmetries, lattice-translational symmetry is discrete so it does not have an associated extensive generator.

Remarkably, despite the special nature of the lattice translational symmetry, we find that there is a formulation of the ETH beyond Eq. (1) that holds in periodic chains. It reads:

$$\begin{aligned} \langle E_m, k_m | \hat{O} | E_n, k_n \rangle &= O(E_m) \delta_{mn} \\ &+ e^{-\frac{S(\bar{E}_{mn})}{2}} f_O(\bar{E}_{mn}, \omega_{mn}, \kappa_{mn}) R_{mn}^O, \end{aligned} \quad (11)$$

where, in addition to the quantities that enter in Eq. (1), it also depends on  $\kappa_{mn} = |k_m - k_n|$ . Notable in Eq. (11) is the lack of dependence of  $O(E_m)$  on  $k_m$  [29], and the lack of dependence of the density of states on the quasimomenta involved, because all quasimomentum blocks asymptotically have the same density of states. For translationally invariant operators  $\hat{O}$ ,  $f_O$  is nonzero only for  $\kappa_{mn} = \Delta_{\ell=0} = 0$ , while for local operators  $\hat{O}^j$  in our chains  $|f_{O^j}|^2$  is  $L$  ( $L/2$ ) times the results in Fig. 4(b) for  $\kappa_{mn} = \Delta_\ell$  with  $\Delta_\ell = 0, \pi$  ( $\neq 0, \pi$ ). In Fig. 4(b) we show results for  $\frac{1}{L}|f_{O^j}|^2$  ( $\frac{2}{L}|f_{O^j}|^2$ ) (symbols) calculated for specific pairs of quasimomenta  $k_m$  and  $k_n$ . We average over 100 pairs of states with  $\bar{E}_{mn} \simeq E_\infty$  and  $\omega_{mn} \simeq \omega$  for several values of  $\omega$ . The results for  $\frac{1}{L}|f_{O^j}|^2$  ( $\frac{2}{L}|f_{O^j}|^2$ ) overlap with the contributions to the spectral function involving all blocks with a given value of  $\Delta_\ell$  in Eq. (10) (see Ref. [21] for further details and results).

*Summary.* We explored the ETH for local and translationally invariant operators in clean chains with OBCs and PBCs. Considering a nonintegrable chain with OBCs (4) in the absence of symmetries, so that the ETH applies to the entire energy spectrum, we showed that the local operator  $\hat{S}_x^j$  at the center of the chain and its translationally invariant counterpart share the same smooth diagonal ETH function. On the other hand, the spectral functions for both observables were found to be different, and this was traced back to correlations between the off-diagonal matrix elements of the local operators  $\hat{S}_x^j$  at different sites. For translational invariant chains with PBCs (3), in which the matrix elements of local operators at different sites are related by translation symmetry, we argued that the spectral functions of local and translationally invariant operators should in general be different. Our findings highlight that, in general, the spectral

functions of local and translationally invariant operators cannot be used interchangeably in clean systems independently of the boundary conditions.

Exploring the quasimomentum dependence of the matrix elements of  $\hat{S}_x^j$  we unveiled an unexpected (due to the lack of an associated extensive generator for the total quasimomentum) extension of the ETH for translationally invariant lattice systems (11). This extension needs to be explored further and opens the door to the simplification of numerical calculations of spectral functions of local operators in translationally invariant systems by only carrying out calculations for  $\lfloor \frac{L}{2} \rfloor + 1$  of the  $L^2$  blocks of the quasimomentum resolved energy spectrum.

*Acknowledgments.* This work was supported by the National Science Foundation (NSF) Grant No. PHY-2309146. The computations were done in the Institute for Computational and Data Sciences Roar supercomputer at Penn State.

---

[1] E. Dagotto, Correlated electrons in high-temperature superconductors, *Rev. Mod. Phys.* **66**, 763 (1994).

[2] M. Z. Hasan and C. L. Kane, Colloquium: Topological insulators, *Rev. Mod. Phys.* **82**, 3045 (2010).

[3] M. Rigol and B. S. Shastry, Drude weight in systems with open boundary conditions, *Phys. Rev. B* **77**, 161101 (2008).

[4] G. Bellomia and R. Resta, Drude weight in systems with open boundary conditions, *Phys. Rev. B* **102**, 205123 (2020).

[5] D. Iyer, M. Srednicki, and M. Rigol, Optimization of finite-size errors in finite-temperature calculations of un-ordered phases, *Phys. Rev. E* **91**, 062142 (2015).

[6] J. M. Deutsch, Quantum statistical mechanics in a closed system, *Phys. Rev. A* **43**, 2046 (1991).

[7] M. Srednicki, Chaos and quantum thermalization, *Phys. Rev. E* **50**, 888 (1994).

[8] M. Srednicki, The approach to thermal equilibrium in quantized chaotic systems, *Journal of Physics A: Mathematical and General* **32**, 1163 (1999).

[9] M. Rigol, V. Dunjko, and M. Olshanii, Thermalization and its mechanism for generic isolated quantum systems, *Nature* **452**, 854 (2008).

[10] L. D'Alessio, Y. Kafri, A. Polkovnikov, and M. Rigol, From quantum chaos and eigenstate thermalization to statistical mechanics and thermodynamics, *Adv. Phys.* **65**, 239 (2016).

[11] L. Foini and J. Kurchan, Eigenstate thermalization hypothesis and out of time order correlators, *Phys. Rev. E* **99**, 042139 (2019).

[12] S. Pappalardi, L. Foini, and J. Kurchan, Eigenstate thermalization hypothesis and free probability, *Phys. Rev. Lett.* **129**, 170603 (2022).

[13] A. Chan, A. De Luca, and J. T. Chalker, Eigenstate correlations, thermalization, and the butterfly effect, *Phys. Rev. Lett.* **122**, 220601 (2019).

[14] C. Murthy and M. Srednicki, Bounds on chaos from the eigenstate thermalization hypothesis, *Phys. Rev. Lett.* **123**, 230606 (2019).

[15] M. Brenes, S. Pappalardi, M. T. Mitchison, J. Goold, and A. Silva, Out-of-time-order correlations and the fine structure of eigenstate thermalization, *Phys. Rev. E* **104**, 034120 (2021).

[16] J. Wang, M. H. Lamann, J. Richter, R. Steinigeweg, A. Dymarsky, and J. Gemmer, Eigenstate thermalization hypothesis and its deviations from random-matrix theory beyond the thermalization time, *Phys. Rev. Lett.* **128**, 180601 (2022).

[17] S. Pappalardi, F. Fritzsch, and T. Prosen, Full eigenstate thermalization via free cumulants in quantum lattice systems, *Phys. Rev. Lett.* **134**, 140404 (2025).

[18] J. D. Noh, T. Sagawa, and J. Yeo, Numerical verification of the fluctuation-dissipation theorem for isolated quantum systems, *Phys. Rev. Lett.* **125**, 050603 (2020).

[19] Note that we use the subindex PBC or OBC to be explicit about the boundary conditions of the Hamiltonian.

[20] L. Capizzi, J. Wang, X. Xu, L. Mazza, and D. Poletti, Hydrodynamics and the eigenstate thermalization hypothesis, *Phys. Rev. X* **15**, 011059 (2025).

[21] See Supplemental Material, where we report results for the spectral functions of the nearest-neighbor correlator, as well as further details and results regarding the quasimomentum resolved contributions to the spectral functions and about the evidence reported in Fig. 4(b) for the ETH in Eq. (11).

[22] M. Pandey, P. W. Claeys, D. K. Campbell, A. Polkovnikov, and D. Sels, Adiabatic eigenstate deformations as a sensitive probe for quantum chaos, *Phys. Rev. X* **10**, 041017 (2020).

[23] T. LeBlond, D. Sels, A. Polkovnikov, and M. Rigol, Universality in the onset of quantum chaos in many-body systems, *Phys. Rev. B* **104**, L201117 (2021).

[24] H. Kim and A. Polkovnikov, Integrability as an attractor of adiabatic flows, *Phys. Rev. B* **109**, 195162 (2024).

[25] M. Abdelshafy, R. Mondaini, and M. Rigol, Onset of quantum chaos and ergodicity in spin systems with highly degenerate Hilbert spaces, *Phys. Rev. B* **112**, L161108 (2025).

[26] M. Mierzejewski and L. Vidmar, Quantitative impact of integrals of motion on the eigenstate thermalization hypothesis, *Phys. Rev. Lett.* **124**, 040603 (2020).

[27] P. Łydżba, R. Świętek, M. Mierzejewski, M. Rigol, and L. Vidmar, Normal weak eigenstate thermalization, *Phys. Rev. B* **110**, 104202 (2024).

[28] T. LeBlond, K. Mallayya, L. Vidmar, and M. Rigol, Entanglement and matrix elements of observables in interacting integrable systems, *Phys. Rev. E* **100**, 062134 (2019).

[29] M. Rigol, Breakdown of thermalization in finite one-dimensional systems, *Phys. Rev. Lett.* **103**, 100403 (2009); Quantum quenches and thermalization in one-dimensional fermionic systems, *Phys. Rev. A* **80**, 053607 (2009).

[30] T. LeBlond and M. Rigol, Eigenstate thermalization for observables that break Hamiltonian symmetries and its counterpart in interacting integrable systems, *Phys. Rev. E* **102**, 062113 (2020).

[31] C. Murthy, A. Babakhami, F. Iniguez, M. Srednicki, and N. Yunger Halpern, Non-abelian eigenstate thermalization hypothesis, *Phys. Rev. Lett.* **130**, 140402 (2023).

[32] J. D. Noh, Eigenstate thermalization hypothesis in two-dimensional  $XXZ$  model with or without  $SU(2)$  symmetry, *Phys. Rev. E* **107**, 014130 (2023).

[33] A. Lasek, J. D. Noh, J. LeSchack, and N. Y. Halpern, Numerical evidence for the non-abelian eigenstate thermalization hypothesis, arXiv:2412.07838.

[34] R. Patil and M. Rigol, Eigenstate thermalization in spin- $\frac{1}{2}$  systems with SU(2) symmetry, Phys. Rev. B **111**, 205126 (2025).

## Supplemental Material: Eigenstate Thermalization for Local versus Translationally Invariant Observables

Rohit Patil and Marcos Rigol

*Department of Physics, The Pennsylvania State University, University Park, Pennsylvania 16802, USA*

### SPECTRAL FUNCTIONS FOR NEAREST-NEIGHBOR CORRELATOR

Here, we provide additional evidence for the difference between the spectral functions of local observables and their translationally invariant counterparts. We consider as the local observable the nearest-neighbor correlator  $\hat{O}^j = \hat{S}_x^j \hat{S}_x^{j+1}$  with  $j = \lceil \frac{L}{2} \rceil$  and its translationally invariant counterpart  $\hat{\mathcal{O}} = \frac{1}{N} \sum_{j=1}^N \hat{S}_x^j \hat{S}_x^{j+1}$ , where  $N = L$  ( $N = L - 1$ ) in chains with PBCs (OBCs).

In Fig. S1, we plot the spectral functions  $|f_{\mathcal{O}}(E_{\infty}, \omega)|^2$  and  $|f_{O^j}(E_{\infty}, \omega)|^2$  for the nearest-neighbor correlator in chains with OBCs [Fig. S1(a)] and PBCs [Fig. S1(b)], respectively. Like for the  $x$ -magnetization in the main text, the spectral functions  $|f_{\mathcal{O}}(E_{\infty}, \omega)|^2$  and  $|f_{O^j}(E_{\infty}, \omega)|^2$  are different for the nearest-neighbor correlator, independently of the boundary conditions. Although, in contrast to the relative ordering  $|f_{\mathcal{O}}(E_{\infty}, \omega)|^2 < |f_{O^j}(E_{\infty}, \omega)|^2$  observed at low frequencies for the  $x$ -magnetization in the main text, we find that  $|f_{\mathcal{O}}(E_{\infty}, \omega)|^2 > |f_{O^j}(E_{\infty}, \omega)|^2$  for the nearest-neighbor correlator. These results are behind our statement in the main text that the relative ordering between  $|f_{\mathcal{O}}(E_{\infty}, \omega)|^2$  and  $|f_{O^j}(E_{\infty}, \omega)|^2$  in general depends on the observable.

In chains with OBCs, the differences between  $|f_{\mathcal{O}}(E_{\infty}, \omega)|^2$  and  $|f_{O^j}(E_{\infty}, \omega)|^2$  can be attributed to the existence of correlations between  $\hat{O}^j$  at different sites. These can be seen in the inset in Fig. S1(a), where we show contributions of different terms in Eq. (7) for  $\hat{\mathcal{O}}$  as a function of distance  $|j - l| \equiv d_{|j-l|}$  between the sites  $j, l$  involved. The nonvanishing results for the terms with  $j \neq l$  ( $d_{>0}$ ) make apparent the existence of correlations between the matrix elements of  $\hat{O}^j$  at different sites.

In chains with PBCs, on the other hand, the differences between  $|f_{\mathcal{O}}(E_{\infty}, \omega)|^2$  and  $|f_{O^j}(E_{\infty}, \omega)|^2$  can be understood in the context of the different terms with  $|k_m - k_n| = \Delta_{\ell}$  in Eq. (10) for the local observable  $\hat{O}^j$ , which breaks the translational invariance of the model and connects eigenstates with different quasimomenta  $k_m, k_n$ . In the inset in Fig. S1(b), we show the contributions for  $\Delta_0$  through  $\Delta_5$  for the local nearest-neighbor correlator  $\hat{O}^j$  considered here. Similar to the results in the main text, the onset of low-frequency plateau moves towards higher frequencies with increasing  $\Delta_{\ell \neq 0}$ .

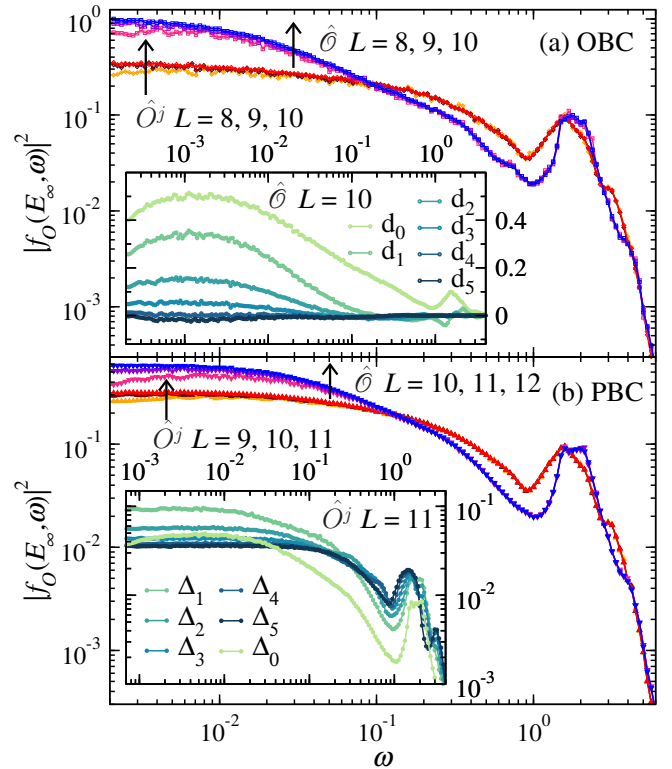


FIG. S1. Spectral functions for the local observable  $\hat{O}^j = \hat{S}_x^j \hat{S}_x^{j+1}$  with  $j = \lceil \frac{L}{2} \rceil$  and its translationally invariant counterpart  $\hat{\mathcal{O}} = \frac{1}{N} \sum_{j=1}^N \hat{S}_x^j \hat{S}_x^{j+1}$  in chains with: (a) OBCs [see Eq. (4)] for which  $N = L - 1$ , and (b) PBCs [see Eq. (3)] for which  $N = L$ . Inset in (a): Contributions to  $|f_{\mathcal{O}}(E_{\infty}, \omega)|^2$ , see Eq. (7) where one needs to change  $L \rightarrow L - 1$ , from terms with  $|j - l| = 0$  through 5 ( $d_0$  through  $d_5$  in the legend) in chains with  $L = 10$ . Inset in (b): Contributions to  $|f_{O^j}(E_{\infty}, \omega)|^2$  from different values of  $\Delta_{\ell}$  in Eq. (10) for  $L = 11$ .

### RESOLVED $(k_m, k_n)$ CONTRIBUTIONS TO FIG. 4(b)

Next, we focus on the local observable  $\hat{O}^j = \hat{S}_x^j$  considered in the main text and show the contribution to  $|f_{O^j}(E_{\infty}, \omega)|^2$  from terms with a given  $\Delta_{\ell}$  resolved by blocks with  $(k_m, k_n)$ . In Fig. S2 we show those contributions from various blocks  $(k_m, k_m + \Delta_{\ell})$  for a given  $\Delta_{\ell}$ , with  $\ell = 1, 2, 3, 4$  [Figs. S2(a)–S2(d)]. Remarkably, the curves for different blocks contributing towards a given

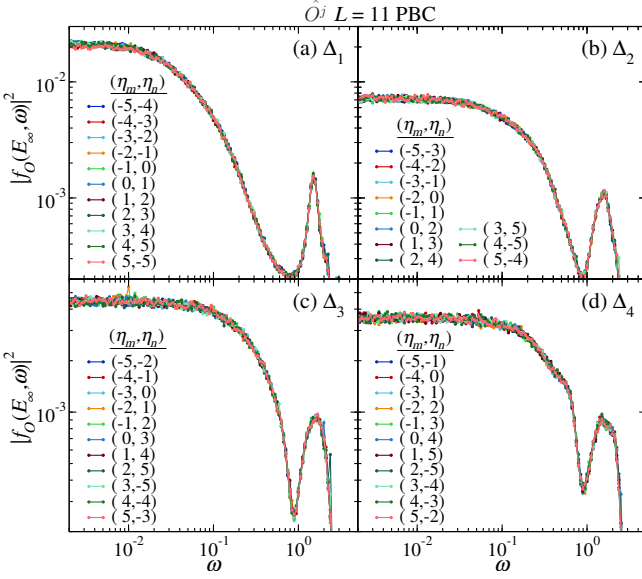


FIG. S2. Contributions from quasimomentum blocks labeled by  $(k_m, k_n) = \frac{2\pi}{L}(\eta_m, \eta_n)$  to the results shown in Fig. 4(b) for different values of  $\Delta_\ell$  with  $\ell = 1, 2, 3, 4$  in (a)–(d), respectively, for  $L = 11$ . See Eq. (10) to understand how those terms enter in the spectral function.

$\Delta_\ell$  collapse signaling the lack of a finer structure at the level of the specific  $(k_m, k_n)$  blocks, with  $|k_m - k_n| = \Delta_\ell$  emerging as the relevant quantity that characterizes the terms in  $|f_{Oj}(E_\infty, \omega)|^2$ . This finding supports our formulation of the ETH in Eq. (11) in the main text.

To test Eq. (11), we calculate the ETH function  $|f_{Oj}(E_\infty, \omega, \Delta_\ell)|^2 \equiv |f_{Oj}(\bar{E}_{mn} \simeq E_\infty, \omega_{mn} \simeq \omega, \kappa_{mn} = \Delta_\ell)|^2$  for  $\kappa_{mn} = \Delta_\ell$  and energies about the center of the spectrum  $\bar{E}_{mn} \simeq E_\infty$  as

$$|f_{Oj}(E_\infty, \omega, \Delta_\ell)|^2 = \frac{D}{L} \overline{|O_{mn}^j|^2}, \quad (\text{S1})$$

where, the factor of  $\frac{D}{L} \approx e^{S(E_\infty)}$  corresponds to the Hilbert space dimension of a  $(k_m, k_n)$  block of the spectrum, and  $\overline{|O_{mn}^j|^2} \equiv \overline{|O_{mn}^j|^2}(\omega)$  is the coarse grained frequency resolved variance of the off-diagonal matrix elements  $O_{mn}^j$ , calculated using 100 pairs of states in the block with  $(k_m, k_n)$  with  $\kappa_{mn} = |k_m - k_n| = \Delta_\ell$ , energy  $|\bar{E}_{mn} - E_\infty| \leq 0.2$  and frequency  $|\log_{10} \omega_{mn} - \log_{10} \omega| \leq 0.01$  for various values of  $\omega$ . From the pairs of states satisfying the above constraints, we select the first 100 pairs of states with the smallest values of  $|\max(E_m, E_n) - E_\infty|$

to calculate the variance  $\overline{|O_{mn}^j|^2}$ .

In Fig. S3 we compare the contributions to  $|f_{Oj}(E_\infty, \omega)|^2$  reported in Fig. 4(b) for different values of  $\Delta_\ell$ , with  $\ell = 1, 2, 3, 4$  [curves in Fig. S3(a)–S3(d)] with the results for the rescaled ETH functions  $\frac{2}{L} |f_{Oj}(E_\infty, \omega, \Delta_\ell)|^2$  (open symbols) calculated within various blocks with  $(k_m, k_m + \Delta_\ell)$ . Note that we need to rescale  $|f_{Oj}(E_\infty, \omega, \Delta_\ell)|^2$  by a factor of  $\frac{2}{L}$  in order to compare with a given  $\Delta_\ell$  contribution to  $|f_{Oj}(E_\infty, \omega)|^2$ , since the latter vanishes because the number of blocks  $(k_m, k_n)$  with  $|k_m - k_n| = \Delta_\ell$  is  $2L$  ( $L$  for  $\Delta_\ell \neq 0, \pi$  ( $\Delta_\ell = 0, \pi$ )), while the total number of blocks is  $L^2$ . This means that their respective contributions vanish as  $\frac{2L}{L^2} = \frac{2}{L}$  ( $\frac{L}{L^2} = \frac{1}{L}$ ) for  $\Delta_\ell \neq 0, \pi$  ( $\Delta_\ell = 0, \pi$ ). It is remarkable that the rescaled ETH functions  $\frac{2}{L} |f_{Oj}(E_\infty, \omega, \Delta_\ell)|^2$  obtained using 100 pairs of energy eigenstates coincides with the contribution to  $|f_{Oj}(E_\infty, \omega)|^2$  obtained using all matrix elements for a given  $\Delta_\ell$ .

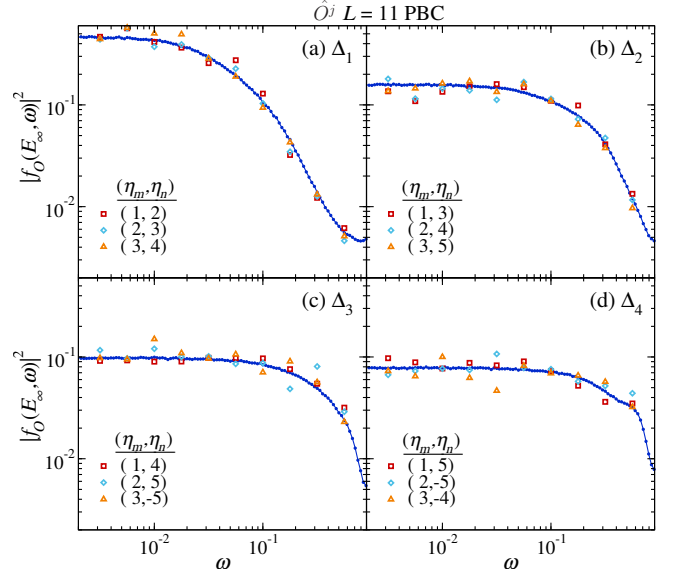


FIG. S3. Contributions to  $|f_{Oj}(E_\infty, \omega)|^2$  shown in Fig. 4(b) for different values of  $\Delta_\ell$  for  $L = 11$ . Open symbols show the rescaled ETH functions  $\frac{2}{L} |f_{Oj}|^2$  in blocks labeled by  $(k_m, k_n) = \frac{2\pi}{L}(\eta_m, \eta_n)$  with  $\eta_m = 1, 2, 3$  and  $k_n = k_m + \Delta_\ell$ , calculated using a coarse grained (frequency resolved) variance of the off-diagonal elements  $|O_{mn}^j|^2$  over 100 pairs of states with  $|\bar{E}_{mn} - E_\infty| \leq 0.2$  and  $|\log_{10} \omega_{mn} - \log_{10} \omega| \leq 0.01$  for values of  $\omega$  separated by  $\delta(\log_{10} \omega) = 0.25$ .